ELSEVIER

Journal of Nuclear Materials 306 (2002) 30–43

journal of nuclear materials

www.elsevier.com/locate/jnucmat

Fuel oxidation and thermal conductivity model for operating defective fuel rods

B.J. Lewis [a,*], B. Szpunar [a], F.C. Iglesias [b]

[a] *Department of Chemistry and Chemical Engineering, Royal Military College of Canada, P.O. Box 17000, Kingston, Ont., Canada K7K 7B4*

[b] *Bruce Power, Fuel and Fuel Channels Nuclear Safety Analysis, and Support Department, 700 University Ave., Toronto, Ont., Canada M5G 1X6*

Received 29 January 2002; accepted 19 August 2002

Abstract

A model has been developed to describe the fuel oxidation behaviour, and its influence on the fuel thermal conductivity, in operating defective nuclear fuel rods. The fuel-oxidation model is derived from adsorption theory and considers the influence of the high-pressure environment that results from coolant entry into the fuel-to-clad gap. This model is in agreement with the fuel-oxidation kinetics observed in high-temperature annealing experiments conducted at 1473–1623 K in steam over a range of pressure from 0.001 to 0.1 MPa. Using a Freundlich adsorption isotherm, the current model is also consistent with recent experiments conducted at a higher pressure of 7 MPa. The model also considers radiolytic effects as a consequence of fission fragment bombardment in the fuel-to-clad gap. This treatment suggests that radiolysis-assisted oxidation is insignificant in operating defective rods (as compared to thermal effects), as supported by limited in-reactor data. The effects of diffusion of the interstitial oxygen ions in the solid in the operating rod is further discussed.

1. Introduction

The release behaviour of fission products from defective rods will depend directly on the fuel oxidation state. More mechanistic theoretical treatments are currently being developed to predict the fuel-oxidation kinetics at high pressure during normal defect operation [1,2]. Fuel oxidation will occur with the presence of steam in the fuel-to-clad gap due to coolant entry through the defect site.

The UO_2 oxidation rate in steam-hydrogen mixtures at high temperature has been extensively studied in out-of-pile experiments, and the data interpreted by simple surface-exchange models in which the kinetics are constrained by equilibrium thermodynamics [1]. Unfortunately, all of these experiments are confined to atmospheric or sub-atmospheric pressures, and may not be pertinent to normal defect operation where the pressures are typically two orders of magnitude greater (i.e., approximately 10 MPa). With operating fuel, there is also a radiation field present where fuel oxidation may result from reaction with highly reactive hydrogen peroxide produced in the gap due to radiolysis of steam by fission-fragment bombardment [3–5]. Moreover, a temperature gradient also arises in operating fuel in contrast to a uniform temperature profile in annealing experiments which can further affect the stoichiometry distribution in the solid fuel matrix. The fuel thermal conductivity is also affected by the stoichiometry profile in the fuel pellet.

With the lack of experimental data, theoretical models based on mechanistic theory can be used to assess these effects. The high-pressure oxidation of the fuel

* Corresponding author. Tel.: +1-613 541 6611; fax: +1-613 542 9489.

E-mail address: lewis-b@rmc.ca (B.J. Lewis).

0022-3115/02/$ - see front matter
PII: S0022-3115(02)01231-X

by steam is treated in this work by adsorption theory. Radiolysis-assisted oxidation is also modelled considering limited experimental observations and energy deposition calculations in the fuel-to-clad gap. Diffusional transport of oxygen ions in the solid fuel is further investigated in this work.

2. Model development

2.1. High-pressure steam oxidation

The fuel oxidation process has been extensively studied at atmospheric pressure where it has been shown that the kinetics are controlled by a reaction at the solid/gas interface and not by the solid-state diffusion of oxygen. In this case, the fuel oxidation kinetics are described by the phenomenological model [6]:

$$c_{\mathrm{U}}\left(\frac{V}{S}\right)_{\mathrm{fuel}}\frac{\mathrm{d}x}{\mathrm{d}t}=c_{\mathrm{U}}\alpha\{x_{\mathrm{e}}-x(t)\}, \tag{1}$$

where c_{U} is the molar density of uranium ($=4.0\times10^{4}$ mol of uranium m^{-3}), α is a surface exchange coefficient ($=0.365\exp\{-23\,500/\mathrm{T(K)}\}$ $\mathrm{m\,s^{-1}}$), x_{e} is the equilibrium stoichiometry deviation, and $(V/S)_{\mathrm{fuel}}$ is the volume-to-surface area ratio of the fuel (m). The value of x_{e} in Eq. (1) is obtained by equating the oxygen potential (i.e., oxygen partial pressure) in the fuel to that in the atmosphere (see Appendix A).

As previously mentioned, the model in Eq. (1) is only specifically valid at atmospheric pressure (since is fitted to the fuel oxidation experiments at this pressure). Therefore, this model cannot necessarily be extrapolated to the high-pressure situation which exists during normal defect operation. In this case, one must appeal to a more mechanistic treatment for extrapolation, such as the Langmuir adsorption theory [9]. For this type of adsorption isotherm, the corresponding relation that describes the oxidation kinetics is given by [1,2,10]:

$$c_{\mathrm{U}}\left(\frac{V}{S}\right)_{\mathrm{fuel}}\frac{\mathrm{d}x}{\mathrm{d}t}=n_{\mathrm{s}}k'_{\mathrm{a}}\frac{A(T)P_{\mathrm{H_2O}}}{1+A(T)P_{\mathrm{H_2O}}}\left[1-\frac{q(x)}{P_{\mathrm{H_2O}}/P_{\mathrm{H_2}}}\right]. \tag{2}$$

Here $n_{\mathrm{s}}=1.66\times10^{-6}$ $\mathrm{mol\,m^{-2}}$ is the density of adsorption sites which assumes a monolayer coverage of 10^{18} $\mathrm{molecules\,m^{-2}}$. In Eq. (2), the oxygen activity $q(x)$ for a gas–solid equilibrium is defined as

$$q(x)=\frac{\sqrt{P_{\mathrm{O_2}}(x)}}{K_{\mathrm{H_2O}}}. \tag{3}$$

For the H_2O decomposition reaction

$$\mathrm{H_2O}\overset{K_{\mathrm{H_2O}}}{\Longleftrightarrow}\mathrm{H_2}+\tfrac{1}{2}\mathrm{O_2} \tag{4}$$

the equilibrium constant in Eq. (3) is evaluated at temperature T (in K) from

$$K_{\mathrm{H_2O}}=\frac{P_{\mathrm{H_2}}\sqrt{P_{\mathrm{O_2}}}}{P_{\mathrm{H_2O}}}=\exp\left\{0.9794\ln T-1.1125-\frac{28\,820}{T}\right\}. \tag{5}$$

In Eq. (2), $P_{\mathrm{H_2O}}$ and $P_{\mathrm{H_2}}$ are the partial pressures (in atm) of steam and hydrogen in the gap atmosphere after dissociation. In fact, using Eqs. (4) and (5), the quantity $q(x)/(P_{\mathrm{H_2O}}/P_{\mathrm{H_2}})$ in Eq. (2) equals $\sqrt{P_{\mathrm{O_2}}(x)/P_{\mathrm{O_2}}}$ where $P_{\mathrm{O_2}}(x)$ pertains to the oxygen partial pressure in the fuel, and $P_{\mathrm{O_2}}$ refers to the oxygen partial pressure in the gap atmosphere (see Appendix A). The parameter $A(T)$ ($\mathrm{atm^{-1}}$) is defined as

$$A(T)=1.0135\times10^{5}\frac{s}{n_{\mathrm{s}}k_{\mathrm{a}}\sqrt{2\pi RTM_{\mathrm{H_2O}}}}, \tag{6}$$

where T is the temperature (in K), $R=8.314$ $\mathrm{J\,mol^{-1}\,K^{-1}}$ and $M_{\mathrm{H_2O}}=18\times10^{-3}$ $\mathrm{kg\,mol^{-1}}$. The desorption rate constant, k_{a}, the steam dissociation rate constant, k'_{a}, and the sticking probability s in the model are obtained with a fitting of Eq. (2) to the predictions of Eq. (1) (at one atmosphere). It is acceptable to use Eq. (1) as a representation of the fuel oxidation experience since it has been validated against numerous experiments at the Chalk River Laboratories (CRL) that were conducted in steam at atmospheric pressure [6]. The resultant kinetics for the models are shown in Fig. 1, using a Runge-Kutta method to solve for $x(t)$ in Eqs. (1) and (2). For the current analysis, the Blackburn model was used to evaluate the oxygen partial pressure in the fuel. An $(S/V)_{\mathrm{fuel}}$ ratio of 330 $\mathrm{m^{-1}}$, typical of a CANDU fuel rod, was also assumed in the calculation. The

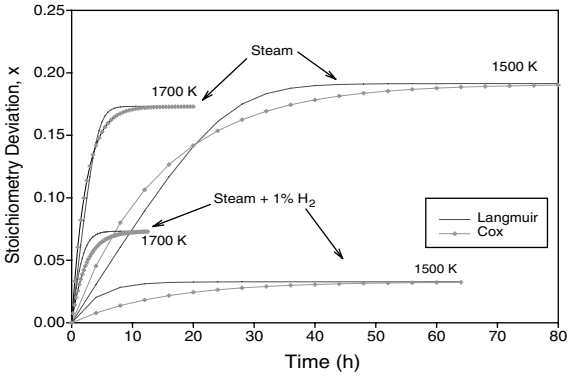

Fig. 1. Comparison of the fuel oxidation kinetics at a pressure of 0.1 MPa (1 atm) in a pure steam and steam-1%H_2 atmosphere at 1500 and 1700 K. The fuel oxidation kinetics are based on a solution of the phenomenological model of Cox et al. in Eq. (1) and the Langmuir adsorption treatment of Eq. (2).

parameters resulting from this fitting are: $k_a = 10^{13}$ $\exp\{-21\,557/T\}$ s^{-1}, $k'_a = 2.48 \times 10^{10}$ $\exp\{-28\,105/T\}$ s^{-1} and $s = 0.023$. This result is comparable with other fittings of Eq. (2) to the available fuel oxidation data [1,2,10]. The fitted value of the desorption rate constant is also consistent for that of a surface-bound species. For instance, the fitted value of the activation energy for k_a (i.e., $\sim$180 kJ mol^{-1}) is typical of that expected for a chemisorption process for H_2O [9]; i.e., this type of process is expected in light of the requirement for a strong adsorbate-substrate bond at high temperature. The pre-exponential factor of 10^{13} s^{-1} for k_a is also a physically accepted value for the vibration frequency of an adsorbed molecule. In addition, the assumption of a single monolayer coverage for n_s is reasonable considering that a monolayer is not normally exceeded with chemisorption.

Without existing data for high-pressure fuel oxidation, one cannot rule out the possibility of a Freundlich isotherm in the adsorption model for the oxidation kinetics [2]. In particular, the surface coverage term for Langmuir adsorption in Eq. (2), i.e.,

$$\theta = \frac{A(T)P_{H_2O}}{1 + A(T)P_{H_2O}} \tag{7}$$

can be replaced by the corresponding Freundlich isotherm [9]:

$$\theta = c_1 P_{H_2O}^{1/c_2} \tag{8}$$

in which $c_2 = 2$ in the present situation. Thus, a similar fitting yields:

$$c_U \left(\frac{V}{S}\right)_{fuel} \frac{dx}{dt} = n_s k'_a \sqrt{P_{H_2O}} \left[1 - \frac{q(x)}{P_{H_2O}/P_{H_2}}\right], \tag{9}$$

where, $k'_a = 1.04 \times 10^9$ $\exp\{-23\,690/T\}$ s^{-1}. As expected, the latter activation energy for k'_a (i.e., 23 690 K) is similar to that for the surface-exchange coefficient in Eq. (1) (i.e., 23 500 K). As shown in Fig. 2, both of the adsorption models are in good agreement with the phenomenological model of Eq. (1) (which is relevant to atmospheric pressure conditions).

Moreover, both of the adsorption models are also able to reproduce the observed oxidation kinetics over the lower pressure range of 0.01–1 atm, where a roughly square-root dependence on the pressure is observed [1,6,10]. For instance, a square-root dependence on the steam pressure is directly observed in Eq. (9) for the Freundlich isotherm. The pressure dependence for the Langmuir model also arises from the surface coverage term in Eq. (7). Thus, in the H_2O/Ar experiments of Albrefah et al. (for steam pressures of 0.25–1 atm at 1623 K) [11], Eq. (6) yields a value of $A = 2.11$ atm^{-1}, and Eq. (7) subsequently predicts a reduction factor for the lower-pressure oxidation kinetics of: $2.11(1)/[2.11(1)+1] \div 2.11(0.25)/[2.11(0.25)+1] = 2.0$. This value is in excellent agreement with an observed square-root dependence of $(1/0.25)^{1/2} = 2.0$. Similarly, for the CEA He/H_2O experiments (i.e., for steam pressures of 0.01–0.03 atm at 1473 K) [6], with $A = 8.56$, a ratio of $\{8.56(0.03)/[8.56(0.03)+1]\} \div \{8.56(0.01)/[8.56(0.01)+1]\} = 2.59$ is obtained. This value is also in good agreement with an observed ratio of $18.2/8.2 = 2.22$ in Fig. 6 of Ref. [6].

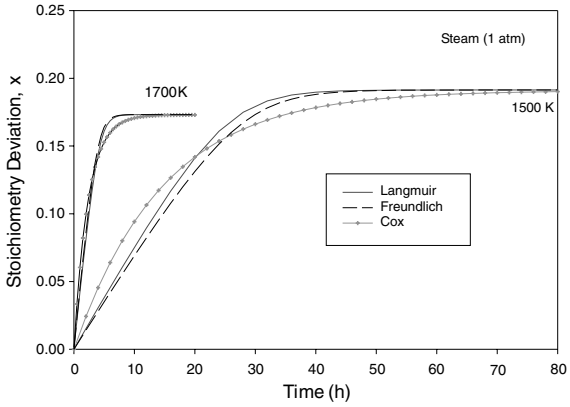

Fig. 2. Comparison of the adsorption isotherm models (Langmuir and Freundlich) versus the phenomenological model of Cox et al. for fuel oxidation in pure steam at a pressure of 0.1 MPa (1 atm) and temperatures of 1500 and 1700 K.

Thus, at atmospheric pressure, all of the models are in relative agreement since they are obtained from a fitting to the available fuel oxidation data at this pressure (see Figs. 1 and 2). In addition, the two adsorption models are able to explain the low pressure kinetics. However, on extrapolation to high pressure, i.e., relevant to defective fuel operation (e.g., 100 atm), a significant deviation occurs (see Fig. 3). For instance, at 1500 K in pure steam, $A = 6.5$ so that $\theta \sim 1$ for a steam pressure of 1 and 100 atm, and hence there is little effect of pressure in Eq. (7).

Therefore, as shown in Fig. 3, both the phenomenological model and the Langmuir model are comparable (i.e., only the equilibrium value of the stoichiometry deviation is slightly affected in these models). On the other hand, there is a direct $\sqrt{P_{H_2O}}$ dependence for the Freundlich isotherm in Eq. (9), resulting in enhanced kinetics by an order of magnitude (i.e., $\sqrt{100}$) (see Fig. 3). In fact, enhanced oxidation kinetics have been observed in experiments at 870 K at a high pressure of 7 and 70 atm, where a square-root dependence on the steam pressure is observed in agreement with the prediction of the Freundlich model [12].

2.2. Radiolysis-assisted fuel oxidation

Since the dose rate due to energy deposition from recoil fission fragments in the steam-filled gap is two

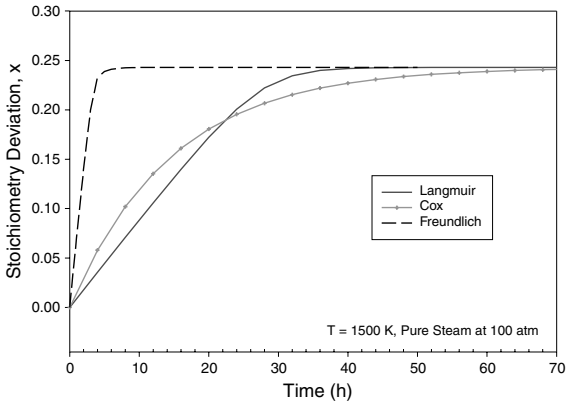

Fig. 3. Comparison of the adsorption isotherm models (Langmuir and Freundlich) versus the phenomenological model of Cox et al. for fuel oxidation in pure steam at a high pressure of 10 MPa (100 atm) and temperature of 1500 K.

orders of magnitude higher than that from fast neutrons or gamma rays, the fission fragments can be considered as the major contributor of steam radiolysis in the fuel-to-clad gap of defective rods [4]. Knockout of particles near the fuel surface, due to elastic collision of primary fragments with stationary oxygen or uranium atoms of the fuel, or with other energetic particles created in a collision cascade, is also a potential process for energy deposition in the gap. However, although there is a greater surface current release, particularly for the higher-order knock-on particles, they have substantially lower energy (i.e., ~200 eV versus 80 MeV for a recoil particle), which results in many orders of magnitude less energy deposition in the gap [13]. Hence, knockout is an inefficient process for the radiolysis reaction compared to that of recoil.

Although many free-radical intermediates are produced, the overall radiolytic reactions are [5]:

$$2H_2O \rightarrow H_2O_2 + H_2 \tag{10a}$$

$$2H_2O \rightarrow O_2 + 2H_2 \tag{10b}$$

The radiolysis products of steam (e.g., H_2O_2 and perhaps O_2) can oxidize the fuel. In particular, the formation of hydrogen peroxide, oxygen and hydrogen greatly exceeds their radically induced recombination rate because of the strong fission fragment radiation field, and therefore the reactions in Eqs. (10a) and (10b) do not reach thermodynamic equilibrium [5,14–16]. The highly reactive hydrogen peroxide molecule, however, can equilibriate with the fuel and oxidize it even in the presence of a large excess of hydrogen [5,14–16]. Although a significant portion of the hydrogen that is liberated in the reactions of Eqs. (10a) and (10b) may result in clad hydriding, it is not clear, however, if this other major radiolysis product could neutralize the tendency of its oxidizing counterparts to increase the stoichiometry of the fuel. Furthermore, as the temperature is raised, radiolytic effects should become insignificant to thermal effects as the thermal reactions and the recombination of transient species become faster [4]. Eventually, at a sufficiently high temperature, the thermal reactions will control the process of fuel oxidation.

Within the current level of uncertainty for the complex radiation chemistry of water vapour, the radiolysis effect can be modelled as a production of equal amounts of H_2O_2 and H_2 in accordance with Eq. (10a) [5]. Since experiments show that H_2O_2 rapidly oxidizes UO_2 even in excess H_2 [17], it can be conservatively assumed that all of the H_2O_2 produced by steam radiolysis is consumed by the fuel-oxidation reaction [5].

2.2.1. Radiolysis production rate

The volumetric rate of production Q^{rad} ($\mathrm{mol\,m^{-3}\,s^{-1}}$) of the radiolytic products is derived as follows. In the fission process, ^{88}Br and ^{135}I can be considered as typical fragments, which obtain 101.5 and 66.5 MeV of the available fission energy at their point of birth in the fuel [13]. As they traverse through the fuel, their energy is lost by electronic and nuclear processes. The average energy of these fragments leaving the UO_2 fuel (of density 10.7 $\mathrm{g\,cm^{-3}}$) can be determined from their energy-range relationships (see Fig. 4(a)) using the SRIM 2000 (stopping and range of ions in matter) code, which is based on a Monte Carlo treatment [18]. As shown in Fig. 4(a), the energy loss, $\mathrm{d}E/\mathrm{d}x$, can be reasonably approximated as a linear function of distance x:

$$\frac{\mathrm{d}E}{\mathrm{d}x} \approx -\left(\frac{2E_0}{r}\right)\left[1-\frac{x}{r}\right], \tag{11a}$$

$$\Rightarrow E(x) = E_0\left[1-\frac{x}{r}\right]^2, \tag{11b}$$

where r is the fission fragment range and E_0 is the initial fission fragment energy (i.e., 101.5 for bromine and 66.5 MeV for iodine). Eq. (11b) follows on integration of Eq. (11a) with the condition, $E(x=0)=E_0$. As shown in Fig. 4(a), a more accurate representation is obtained if the average range plus its straggling is used in Eq. (11a) (i.e., $r_{\mathrm{Br\text{-}88}} = 8.70 + 0.68\ \mu\mathrm{m} = 9.38\ \mu\mathrm{m}$ and $r_{\mathrm{I\text{-}135}} = 6.43 + 0.76\ \mu\mathrm{m} = 7.19\ \mu\mathrm{m}$) instead of just the average range itself [18]. The same relationship in Eq. (11b) has been proposed in Ref. [4]. Thus, the average energy $\langle E\rangle$ of the fission fragments leaving the UO_2 is simply obtained on use of Eq. (11b) where by definition:

$$\langle E\rangle = \int_0^r E(x)\,\mathrm{d}x \Big/ \int_0^r \mathrm{d}x = \frac{E_0}{3}. \tag{12}$$

Therefore, a fragment with an initial energy E_0 will be reduced by a factor of 3 (on average) as it enters into the

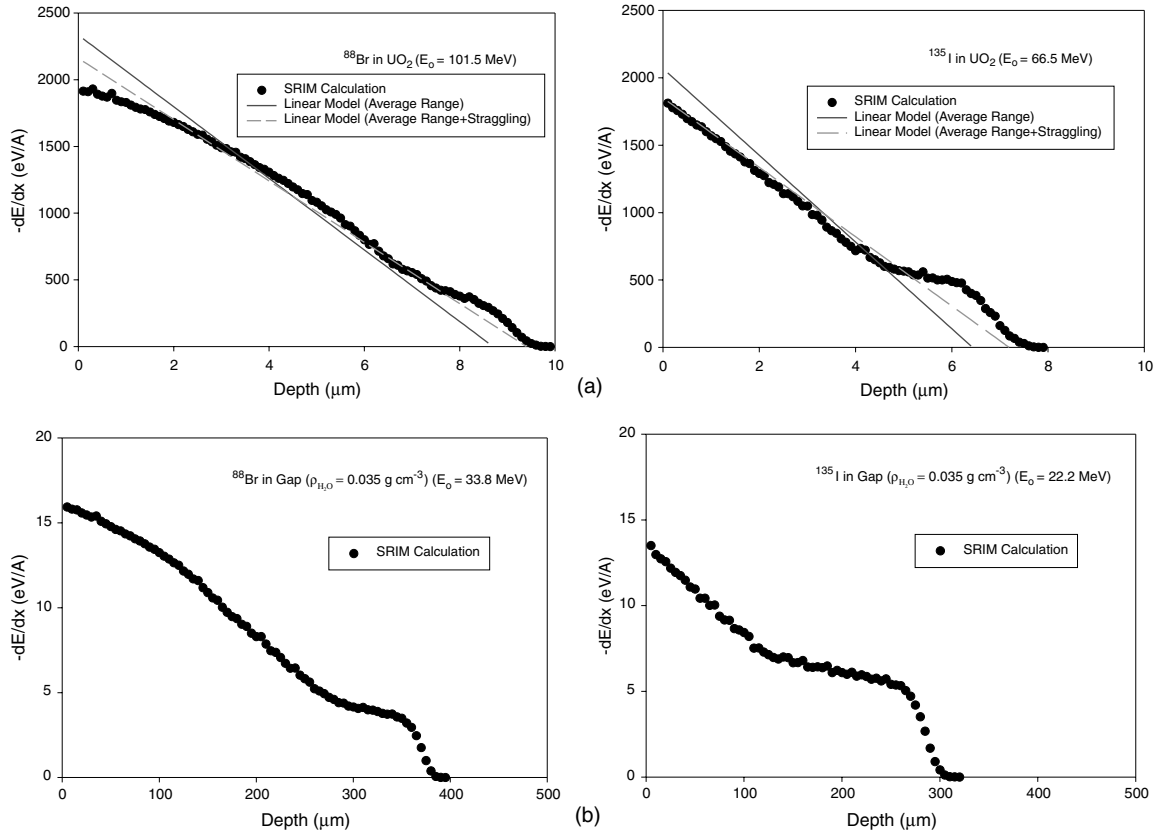

Fig. 4. Energy loss of fission fragments ^{88}Br and ^{135}I in the (a) UO_2 fuel and (b) steam-filled fuel-to-clad gap. A linear energy loss approximation for the slowing down of the fission fragments in the UO_2 is also shown.

fuel-to-clad gap. The high-energy fission fragments subsequently traverse through the thin annular gap of thickness $h \sim 12.5$ μm (i.e., for CANDU fuel) with a mean chord length $\bar{z} = 2h = 25$ μm [13]. As shown in Fig. 4(b), with the gap filled with steam at a density of 0.035 g cm^{-3}, only a small amount of energy loss occurs as the fragments eventually embed themselves in the adjacent clad wall. Although the gap size in operating LWR fuel rods is ~4 times larger (since the clad is free standing), the released fission fragments are similarly embedded in the adjacent clad wall.

Hence, the rate of production Q_j^{rad} (mol m^{-3} s^{-1}) due to steam radiolysis of molecule j (i.e., hydrogen or hydrogen peroxide) per unit volume in the gap is given by

$$Q_j^{\text{rad}} = \frac{q_{\text{H}_2\text{O}} G_j \bar{z}}{N_{\text{Av}} V_{\text{gap}}} \sum_{\text{i=I,Br}} \left[\frac{1}{4} r_i S \dot{F} \right] \text{LET}_i. \tag{13}$$

The quantity in square brackets is the familiar recoil release rate of fission fragments from a solid fuel body [3]. Here N_{Av} is Avogadro's number ($= 6.022 \times 10^{23}$ molecule mol^{-1}), $\bar{z}$ is the path length in the gap (m), r_i is the fission fragment range in the fuel ($= 9.38 \times 10^4$ Å for ^{88}Br and 7.19×10^4 Å for ^{135}I), S is the surface area of the fuel (m^2), V_{gap} is the gap volume (m^3), $\dot{F}$ is the fission rate density (fission m^{-3} s^{-1}) and LET is the fission fragment linear energy transfer (eV Å^{-1}). As a conservative calculation for the radiolysis analysis, the energy loss by bremsstrahlung radiation can be neglected so that the energy absorbed in the steam is equal to the energy loss in the gap [19]. Therefore, in Eq. (13), $\text{LET} = (\text{d}E/\text{d}x)_{\text{loss}}$, where the average energy loss in the gap over the given path length $\bar{z}$ is evaluated from Fig. 4(b) as $(\text{d}E/\text{d}x)_{\text{loss}}^{\text{Br-88}} \approx 15.7$ eV Å^{-1} and $(\text{d}E/\text{d}x)_{\text{loss}}^{\text{I-135}} \approx 12.8$ eV Å^{-1}. The parameter G_j is the G-value for the radiation yield of molecule j produced per 100 eV of ionizing energy deposited by the fission fragments in the water vapour molecules of the gas mixture. Here, the gas mixture in the gap has a steam mole fraction $q_{\text{H}_2\text{O}}$. Boyd and Miller studied fission fragment radiolysis of water vapour with and without various additives as a function of temperature (170–365 °C) and density (1–50 mg ml^{-1}) [20]. Based on this work, McCracken suggested a G-value ≈ 6.5/100 eV for oxidizing or reducing equivalents in water vapour in order to reflect the probable occurrence of impurity (uranium) species in the gap and

possible reactions with the inner clad surface [4]. This value is also supported by the recent experimental work of Olander et al., where $G \sim 8.5/100$ eV for the H_2 radiolysis product with α-particle radiation in pure saturated steam at 70 atm [5,17]. Thus, in the present analysis, in accordance with Eq. (10a), it can be assumed that $G_{H_2} = G_{H_2O_2} = G \approx 6.5/100$ eV.

Since the experiments show that H_2O_2 rapidly oxidizes the UO_2, even in the presence of excess H_2, it can be assumed that all of the H_2O_2 produced by radiolysis is consumed in the fuel oxidation process. Thus, by neglecting gas phase recombination reactions involving H_2O_2 and the loss of this species by cladding corrosion, this assumption will yield an upper limit of the radiolytically driven fuel oxidation rate. Hence, the rate at which the H_2O_2 is consumed per unit surface area of fuel is given by $R^{ox}_{H_2O_2}$ (in mol $m^{-2}\,s^{-1}$):

$$R^{ox}_{H_2O_2} = hQ^{rad} = \frac{q_{H_2O} G \bar{z} \dot{F}}{4N_{Av}} \sum_{i=I,Br} \left[r \left(\frac{dE}{dx} \right)_{loss} \right]_i . \tag{14}$$

2.2.2. Fuel oxidation kinetics

The rate at which the fuel oxidizes is governed by the difference between the rates of oxidation by steam and hydrogen peroxide, and reduction by hydrogen. The thermodynamic model of Eqs. (1), (2) or (9) accounts for the fuel oxidation and reduction reaction rates in the presence of a gaseous mixture of hydrogen and steam. This process is limited by a thermodynamic constraint that stops the reaction when the equilibrium stoichiometry deviation is reached (see Figs. 1–3). In contrast, the (maximum) radiolytically driven fuel oxidation rate in Eq. (14) is not thermodynamically limited. Hence, the conservation equation for the oxygen balance in the fuel is [5,17]:

$$c_U \left(\frac{V}{S} \right)_{fuel} \frac{dx}{dt} = R^{ox}_{H_2O_2} + R^{ox}_{H_2O} - R^{red}_{H_2}, \tag{15}$$

where

$$R^{ox}_{H_2O} - R^{red}_{H_2} = f(T, P_{H_2O}) \left\{ 1 - \sqrt{P_{O_2}(x)/P_{O_2}} \right\}. \tag{16}$$

Here the function $f(T, P_{H_2O})$ depends on the choice of the adsorption isotherm,

$$f(T, P_{H_2O}) = \left\{ \begin{array}{ll} n_s k'_a \frac{A(T) P_{H_2O}}{1 + A(T) P_{H_2O}} & \text{(Langmuir)} \\ n_s k'_a \sqrt{P_{H_2O}} & \text{(Freundlich)} \end{array} \right\}. \tag{17}$$

Alternatively, at atmospheric pressure, Eq. (1) can also be used for $R^{ox}_{H_2O} - R^{red}_{H_2}$. For the oxygen balance of Eq. (15), it has been implicitly assumed that the rate of fuel oxidation by hydrogen peroxide gas results from the reaction [17]:

$$H_2O_2(g) \rightarrow O(s) + H_2O(g) \tag{18}$$

where O(s) represents oxygen in the solid fuel above the normal O/U ratio of two. The quantities of $P_{O_2}(x)$ and P_{O_2} in Eq. (16) are evaluated with the models in Appendix A, considering the initial quantities of H_2O and H_2 in the gap atmosphere prior to dissociation.

Eq. (15) can be used to assess the fuel oxidation kinetics in the CRL experiment, FFO-103, where a CANDU-size fuel rod was machined with 23 slits along the entire length of the cladding [3]. This experiment was designed to minimize the holdup of fission products in the fuel-to-clad gap, and to permit unrestricted coolant entry so as to maximize the fuel oxidation. The defected fuel rod operated in-reactor at a linear power of ~50 kW m^{-1} (i.e., a fission density rate of 1.35×10^{19} fission $m^{-3}\,s^{-1}$) in a pressurized water loop at 10 MPa. Based on an analysis with the ELESIM fuel performance code (using the MATPRO.11 thermal conductivity correlation for hyperstoichiometric fuel), the experimental rod had an average fuel temperature of ~1550 K (see also discussion in Section 2.2.3) [21]. In this analysis, it can be assumed that the gap is essentially filled with pure steam, implying an oxygen partial pressure of 3.23×10^{-3} atm (see Appendix A). The solution of the fuel oxidation model in Eqs. (14)–(16) (with the two adsorption isotherms) is shown in Fig. 5, with and without radiolysis-assisted fuel oxidation. When coolant radiolysis is taken into consideration with the Langmuir adsorption isotherm, the kinetics are more rapid and a slightly higher equilibrium stoichiometry deviation results. However, as previously discussed, the Freundlich isotherm is more appropriate to describe the high-pressure fuel oxidation behaviour and in this case radiolysis does not significantly enhance the oxidation kinetics.

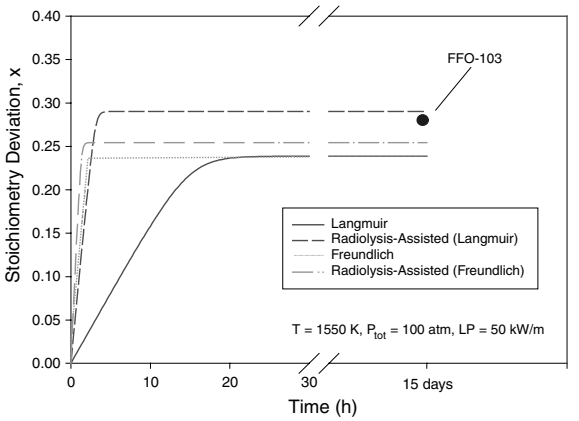

Fig. 5. Comparison of the predicted fuel oxidation kinetics (with and without radiolysis-assisted oxidation) with experiment FFO-103.

An equilibrium stoichiometry deviation of 0.276 was measured by gravimetric analysis after 15 d of operation in experiment FFO-103 (see Fig. 5) [3]. This measured value is in reasonable agreement with that predicted by equilibrium thermodynamics (using the Blackburn model in Appendix A) for steam oxidation (i.e., 0.24). Interestingly, the oxidation/reduction in Eq. (16) actually limits the overall equilibrium stoichiometry deviation in Eq. (15). Here, the increased $P_{O_2}(x)$ is eventually higher than the value of the atmospheric P_{O_2} (for pure steam) in Eq. (16) so that a reduction actually occurs (i.e., $R^{ox}_{H_2O} - R^{red}_{H_2} < 0$). Thus, this resulting negative term is eventually balanced by the radiolysis term in Eq. (15) so that an equilibrium oxidation situation is established. This equilibrium situation is rapidly reached as shown in Fig. 5. The Freundlich model prediction is also consistent with the observed fission product release behaviour, where a relatively constant release rate was quickly achieved over the course of the experiment for those isotopes that had reached radioactive equilibrium [3].

For typical defective rods, where the coolant entry is more limited, hydrogen liberated in the oxidation reactions will reduce the oxygen potential in the gap and hence the amount of fuel oxidation. The steam must also diffuse into the gap as a source from the defect site. Thus, under normal defect occurrences, the P_{O_2} in Eq. (16) must be evaluated for the relevant hydrogen/steam mixture in the gap [2].

2.2.3. Oxygen transport in the solid fuel

In most high-temperature annealing experiments, the fuel is heated in a furnace producing a constant temperature across the pellet. This out-of-pile heating method will yield a uniform oxygen concentration distribution in the solid fuel. On the other hand, during in-reactor operation, a temperature profile develops due to the internal fission heating. As such, if the steam delivery is only to the external surface of the pellet via gap transport, the surface temperature of the pellet is too low during normal operation to provide sufficiently rapid kinetics to yield the oxidation state that is normally observed in defective rods [12]. However, the gas present in the gap can penetrate through cracks in the pellet by gas phase transport and react with the fuel at temperatures much higher than the fuel surface temperature [21]. Consequently, an oxygen profile will develop in the fuel pellet since the thermodynamics of the oxidation reaction is temperature dependent. In particular, Olander et al. have proposed a complicated delivery mechanism involving a two-zone transport/reaction model for fuel oxidation in which the H_2O/H_2 gas mixture in the gap diffuses radially through a network of cracks to a central reaction zone where the kinetically-limited oxidation of the fuel occurs [12]. The reaction products that consist of H_2 in the gas in the cracks and interstitial oxygen ions in the solid fuel are then transported by diffusion in their respective phases back to the pellet periphery. The outer pellet surface however is assumed to remain stoichiometric in the model.

In reality, transport in the gas phase is much more rapid than that of solid state diffusion so that it can be assumed that the cracks in the fuel act as a continuous supply of H_2O/H_2 from the gap [21]. However, as a result of the temperature profile in the fuel, an oxygen concentration profile will develop that can lead to a redistribution of the interstitial oxygen ions up the temperature gradient via radial diffusion. In this situation, the kinetic model of Eq. (1) can be modified, where from a mass balance for the cylindrical fuel pellet of radius a:

$$c_U \frac{dx}{dt} = c_U \alpha (P_{H_2O})^{1/2} \left(\frac{S}{V}\right)_{fuel} \{x_e - x(t)\} + \frac{c_U}{r}\left[\frac{\partial}{\partial r}\left(Dr\frac{\partial x}{\partial r}\right)\right], \tag{19}$$

where D is the solid state diffusion coefficient for the interstitial oxygen transport in the solid fuel. The simple phenomenological model of Eq. (1) has been assumed in Eq. (19) however a factor of $\sqrt{P_{H_2O}}$ has been added to account for high pressure in accordance with the Freundlich adsorption theory (see Section 2.1). Eq. (19) is subject to the following initial and boundary conditions. The fuel pellet is initially assumed to be stoichiometric:

$$x = 0, \quad 0 \leqslant r \leqslant a, \quad t = 0. \tag{20a}$$

A reflexive boundary condition follows at the centre of the pellet ($r = 0$) due to symmetry:

$$\frac{\partial x}{\partial r} = 0, \quad r = 0, \quad t > 0. \tag{20b}$$

At the surface of the pellet, the stoichiometry $x(r = a)$ is set equal to the value of x which is established as a result of an equilibrium between the solid fuel and the gap atmosphere, where on solution of Eq. (1) (accounting for high pressure effects):

$$x = x_e\left[1 - \exp\left(-\frac{S}{V}\sqrt{P_{H_2O}}\alpha t\right)\right], \quad r = a, \ t > 0. \tag{20c}$$

In fact, due to the lower temperature at the fuel surface, the fuel essentially remains stoichiometric at this location (i.e., $x \approx 0$ at $r = a$, $t > 0$).

The diffusion coefficient for oxygen in Eq. (19) should correspond to that for chemical diffusion rather than for self-diffusion since it determines the movement of oxygen ions in the presence of an oxygen concentration gradient as opposed to that of self diffusion which applies to simple random Brownian motion for a fuel sample with a homogeneous stoichiometry [22]. The chemical diffusion coefficient is much less dependent on

stoichiometry and can be represented by the simple Arrhenius form [22]:

$$D = 2.5 \times 10^{-4} \exp\left(-\frac{16400}{T}\right) \text{ m}^2\,\text{s}^{-1}. \quad (21a)$$

Eq. (21a) is an average over the stoichiometry range $10^{-5} \leqslant x \leqslant 10^{-1}$ and is specifically valid for a temperature range of $700 \leqslant T \leqslant 1800$ K [22]. Recent measurements of the chemical diffusion coefficient at 1000 K (i.e., 2.5×10^{-11} m^2 s^{-1} at $x \sim 0.002$ and 5.6×10^{-12} m^2 s^{-1} at $x \sim 0.12$) [23] are in good agreement with the predictions of Eq. (21a) which yields a value of 1.89×10^{-11} m^2 s^{-1}. By comparison, the diffusion coefficient for oxygen self-diffusion in hyperstoichiometric uranium dioxide is given by a best fit equation to all available data as [22]:

$$D_0 = 3.82 \times 10^{-5} \times \left\{x + \left[x^2 + 0.464 \exp\left(-\frac{26700}{T}\right)\right]^{1/2}\right\} \times \exp\left(-\frac{16500}{T}\right) \text{ m}^2\,\text{s}^{-1}, \quad (21b)$$

which is valid for the same temperature range and a stoichiometry range of 0–0.2. Over typical fuel operating temperatures and stoichiometries, Eq. (21a) yields significantly larger values compared to that of Eq. (21b) and therefore only chemical diffusion will be included in our calculations.

For a solution of Eq. (19), the temperature profile must also be known as follows from a solution of the steady state heat conduction equation [24]:

$$\frac{1}{r}\frac{\mathrm{d}}{\mathrm{d}r}\left(rk\frac{\mathrm{d}T}{\mathrm{d}r}\right) + H\left[\frac{(\kappa a)}{2I_1(\kappa a)}\right] I_0(\kappa r) = 0. \quad (22)$$

Here k is the thermal conductivity, which is a function of both temperature T and the fuel stoichiometry deviation x that depend on the radial position r. The second term in Eq. (22) is the volumetric heat generation rate which takes into account the effect of flux depression. The parameter H is related to the linear power P of the fuel rod such that $H = P/(\pi a^2)$ and κ is the inverse neutron diffusion length (which is taken equal to 1.1 cm^{-1} for naturally-enriched fuel at a burnup of 8000 MWd/t). Similarly, Eq. (22) is subject to the boundary conditions [24]:

$$\frac{\mathrm{d}T}{\mathrm{d}r} = 0, \quad r = 0 \quad (23a)$$

and

$$T = T_s, \quad r = a, \quad (23b)$$

where T_s is the fuel surface temperature.

2.2.3.1. Fuel thermal conductivity. In order to determine the temperature distribution in uranium oxides, the thermal conductivity of the fuel must be known. The urania is a Mott insulator in which heat can be transferred by both radiation (photons) and by conduction via lattice vibration (phonons) and electron–hole movement (polarons).

The radiative contribution to the thermal conductivity is typically less important at normal fuel operating temperatures as given by [25]:

$$k_{\text{rad}} = 1.5 \times 10^{-10}\left[\frac{N^2}{\alpha_R(T)}\right] T^3 \text{ kW m}^{-1}\,\text{K}^{-1}. \quad (24a)$$

The index of refraction N can be taken to be independent of temperature and wavelength and set equal to 2.25, and

$$\alpha_R(T) = C_1 \exp(C_2 \times T), \quad (24b)$$

with $C_1 = 8750$ m^{-1} and $C_2 = 7.5971 \times 10^{-4}$ K^{-1}.

The phonon contribution to the thermal conductivity k_{ph} is generally the dominant component as represented by [26]:

$$k_{\text{ph}} = \frac{1}{A(x) + B(x)T} \quad \text{kW m}^{-1}\,\text{K}^{-1}, \quad (25a)$$

where

$$A(x) = 14 - 10.763\sqrt{x} - 2381.4x + 12819.86(\sqrt{x})^3 - 14000x^3 \quad (25b)$$

and

$$B(x) = \begin{cases} 0.2218 + 0.2562\sqrt{x} - 0.64x - 3.6764(\sqrt{x})^3, \\ \quad x < 0.155, \\ 0, \quad x \geqslant 0.155. \end{cases} \quad (25c)$$

For numerical computations, Eq. (25c) can be equivalently replaced by a single equation (which avoids the difficulty of a negative B value):

$$B(x) = 0.2218 + 0.2562\sqrt{x} - 0.64x - 3.6764(\sqrt{x})^3 + 17.3x^3 \quad (25d)$$

The parameter A in Eq. (25b) has been slightly modified from the original analysis in Ref. [26] in order to predict the central melting that was observed in the lower part of the fuel rod in experiment FFO-103 at a linear power rating of 52 kW m^{-1} (see the following discussion and Fig. 8) [27]. However, as shown in Fig. 6(a), the correlation in Eq. (25b) is in good agreement with other available data and theoretical predictions [26,28–34]. As suggested in Ref. [26] and shown in Fig. 6(b), the correlation for B in Eq. (25c) is only allowed to take on positive values and is in good agreement with the literature data [28–30]. The 95% confidence limits for the model fittings to the data are also shown in Figs. 6(a)

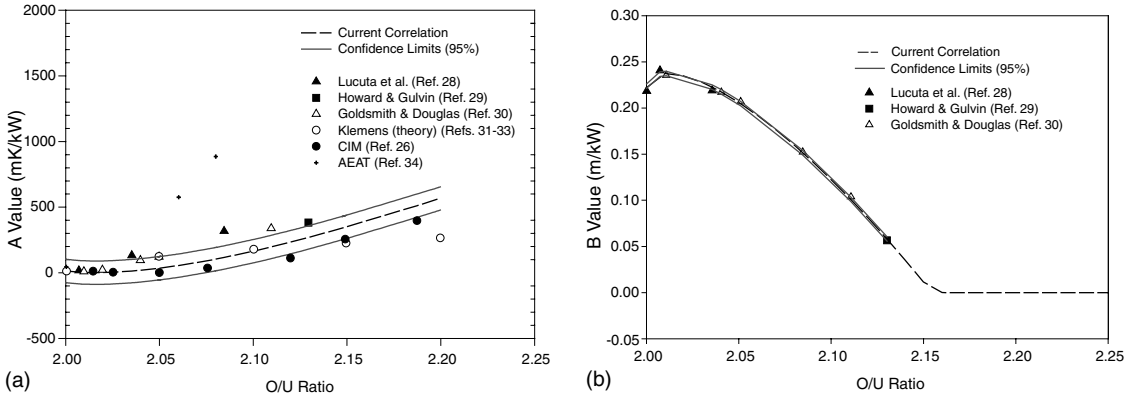

Fig. 6. Variation of the parameters (a) A in Eq. (25b) and (b) B in Eq. (25c) with fuel stoichiometry.

and (b). In particular, the larger spread in the confidence limit of Fig. 6(a) permits the introduction of a bias in Eq. (25b) from the original model fitting of Ref. [26].

The third contribution to the thermal conductivity arises from electron–hole (polaron) transport, which becomes more important at a higher temperature and a lower stoichiometry deviation [25]:

$$k_{\mathrm{e}} = \left(\frac{k_{\mathrm{B}}}{e}\right)^2 T \frac{\sigma_{\mathrm{e}}\sigma_{\mathrm{h}}}{\sigma_{\mathrm{e}}+\sigma_{\mathrm{h}}} \left(\frac{\Delta U}{k_{\mathrm{B}}T}\right)^2. \tag{26}$$

Here k_{B} is the Boltzman constant, e is the electron charge, σ_{e} is partial dc electric conductivity due to electron transport, σ_{h} is the partial dc electric conductivity due to the hole transport and ΔU is the Mott–Hubbard energy gap. Eq. (26) can be further developed as [25,35]:

$$k_{\mathrm{e}} = C_\sigma \left(\frac{\Delta U}{k_{\mathrm{B}}T}\right)^2 \frac{np(1-n-p)}{n+p} \mathrm{e}^{-\Delta E/(k_{\mathrm{B}}T)} \ \mathrm{kW\,m^{-1}\,K^{-1}}, \tag{27a}$$

where $C_\sigma = 3.71 \times 10^{-3}$ kW m^{-1} K^{-1}, ΔU is the Mott–Hubbard energy gap $= 4.33 \times 10^{-19}$ J, and ΔE is the electron mobility activation energy $= 4.81 \times 10^{-20}$ J [25,36]. The molar electron (n) and hole (p) concentrations can be determined from conditions of electroneutrality and thermodynamic equilibrium, where for a given stoichiometric deviation x:

$$p = x + \frac{-2\gamma + \sqrt{x^2(1-4\gamma)+\gamma}}{1-4\gamma}, \tag{27b}$$

$$n = p - 2x, \tag{27c}$$

$\gamma = \exp\{-\Delta F/(k_{\mathrm{B}}T)\}$, $\Delta F = \Delta U - T\Delta S$ and $\Delta S = 2.62 \times 10^{-23}$ J K^{-1} [25,36].

Thus, the overall thermal conductivity which results from the three contributions in Eqs. (24a), (24b), (25a), (25b), (25d), and (27a)–(27c) is given collectively by (see Fig. 7):

$$k = k_{\mathrm{ph}} + k_{\mathrm{e}} + k_{\mathrm{rad}}. \tag{28}$$

Fig. 7 depicts the total thermal conductivity in Eq. (28), and the dominant phonon contribution in Eqs. (25a), (25b) and (25d). The thermal conductivity is reduced with increasing stoichiometry but becomes less dependent on temperature.

2.2.3.2. Fuel temperature and stoichiometry deviation profile. To calculate the temperature profile in an operating fuel rod, Eqs. (19), (20a)–(20c), (21a), (22), (23a), (23b), (25a), (25b), (25d), (27a)–(27c) and (28) are solved iteratively using a finite difference approach. For the thermal conductivity contributions only the phonon and polar components are considered in this calculation (since the radiation component is typically small and has a large uncertainty). As an example, Figs. 8(a) and (b) show the temperature and stoichiometry deviation

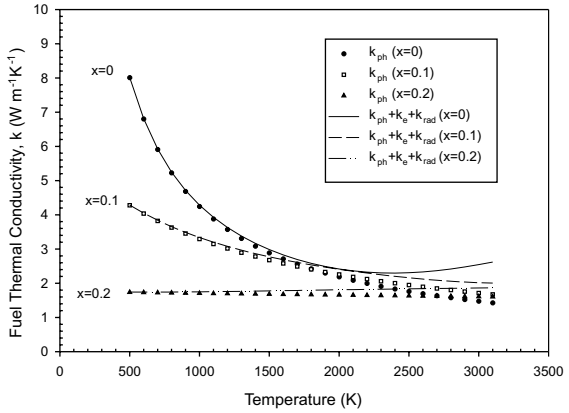

Fig. 7. Urania thermal conductivity (at zero burnup) as a function of temperature and stoichiometry deviation.

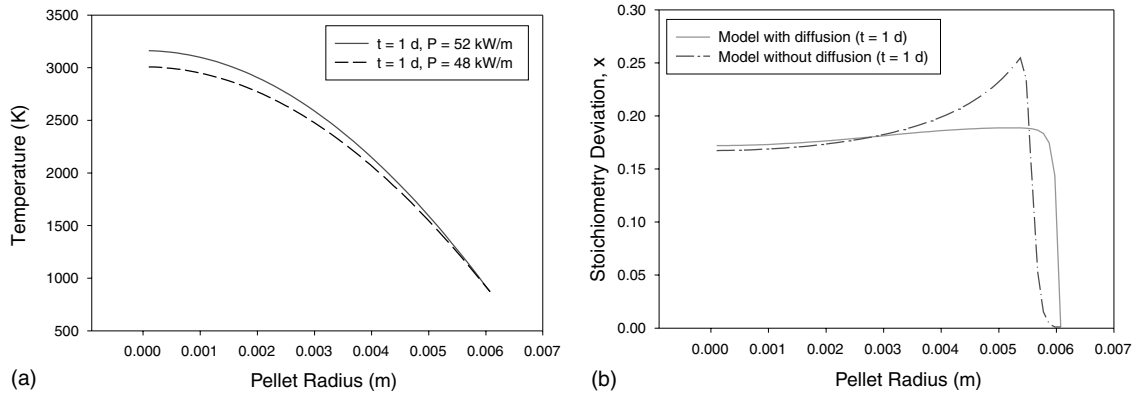

Fig. 8. (a) Predicted fuel temperature profile, and (b) stoichiometry deviation profile with and without diffusion of oxygen in the solid. The development of the temperature profile in (a) depends specifically on the stoichiometry profile in (b) (i.e., thermal conductivity in the solid) as depicted after 1 d of irradiation. The calculations in (b) correspond to a defective CANDU fuel rod operating at a linear power of 52 kW m^{-1} in which pure steam is present in the gap atmosphere.

profile for a defective CANDU-size fuel rod with an $(S/V)_{\text{fuel}}$ ratio of 330 m^{-1}. This analysis is representative of experiment FFO-103 where the bottom section of the defective rod operated at a maximum linear rating of 52 kW m^{-1} with a surface fuel temperature of 870 K [21]. It is also assumed that there is a pure steam atmosphere in the gap since the rod had 23-machined slits along the entire length of the cladding. Consequently, the fuel thermal conductivity was degraded due to significant fuel oxidation which led to central fuel melting as predicted in Fig. 8(a) and observed in Fig. 9. The current analysis in fact predicts a much greater degradation in the fuel conductivity than that simulated with the MATPRO.11 correlation in the analysis of Ref. [21]. Also, in agreement with experiment, no central melting is predicted in Fig. 8(a) at the mid-plane section of the rod that had operated at 48 kW m^{-1}. As shown in Fig. 8(b), a volumetrically averaged O/U ratio of 2.18 is calculated for one day of irradiation (i.e., where the curves in Fig. 8 have already reached a steady state distribution in this period of time). This theoretical result is comparable to a reported value of 2.276 as determined by gravimetric analysis at the mid-plane section of the rod following the 15-day test. This slight discrepancy in the O/U ratio may be somewhat attributed to the neglecting of radiolysis effects in the fuel oxidation calculation (see Section 2.2.2), the uncertainty in the Blackburn thermochemical model and for the gravimetric measurement technique, and the possible air oxidation of the defective fuel rod during the post-test examination in the hot cell.

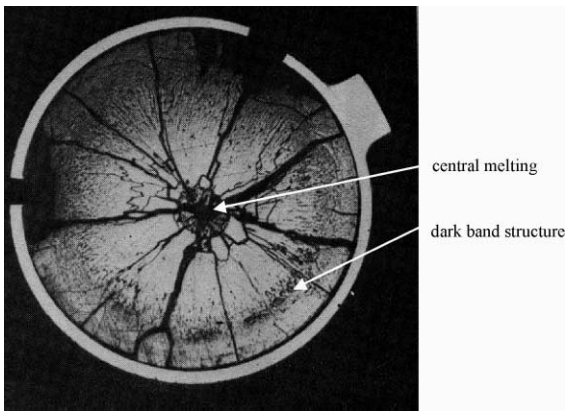

Fig. 9. Post irradiation examination of the defective rod in experiment FFO-103 showing central melting and a dark band structure near the surface of the pellet.

It can been seen in Fig. 8(b) that oxygen diffusion does not significantly affect the stoichiometry deviation profile except towards the surface of the pellet where it tends to flatten out. In fact, the shape of the stoichiometry deviation profile in Fig. 8(b), in which oxygen diffusion is considered in the model, is similar to that predicted with the more complex treatment of Olander in Ref. [12]. On the other hand, as shown in Ref. [21] and depicted in Fig. 8(b) for the curve in which oxygen diffusion is neglected, the resultant simple thermodynamic model is able to predict the occurrence of an oxide phase higher than U_4O_9 ($x = 0.25$) in a thin band near the outer region of the pellet. Interestingly, the radial location of this higher oxide corresponds precisely to the position of a dark band feature observed in the post-irradiation metallography of Fig. 9 [27]. This feature is generally observed in the metallography of defective fuel rods. However, it has been suggested that this banding structure may be related to the presence of bubbles [37]. With a reduction in the chemical diffusion coefficient in the current model, the stoichiometry deviation profile

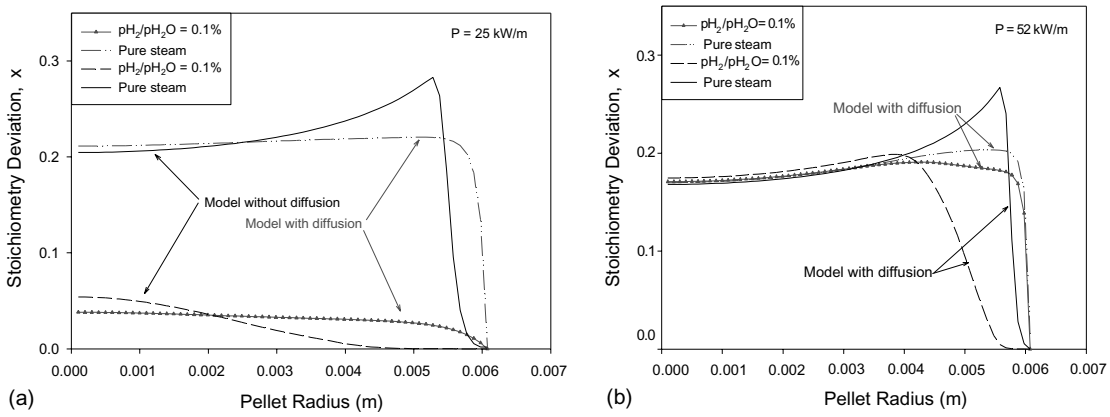

Fig. 10. Stoichiometry deviation profile with and without diffusion of oxygen in the solid for different atmospheric oxygen potentials in the fuel-to-clad gap at (a) 25 kW m^{-1} and (b) 52 kW m^{-1}.

tends to peak in a small region near the outer surface of the pellet where the banding is observed to occur. In addition, near the centre of the pellet where there is less of an oxygen concentration gradient, the use of a self diffusion coefficient in the model (Eq. (21b)) may be more appropriate.

In defective fuel rods with typical-sized failures, hydrogen generated by oxidation of the fuel and clad must counter-diffuse against incoming steam that enters through the remote defect site. The presence of this hydrogen will affect the local oxygen potential in the fuel-to-clad gap and thus the stoichiometry deviation in the fuel. For instance, the stoichiometry deviation profile that arises with pure steam or a hydrogen-to-steam partial pressure ratio of $P_{H_2}/P_{H_2O} = 0.1\%$ is shown in Fig. 10 at different linear heat ratings. The influence of oxygen diffusion in the model is also shown. Interestingly, with the presence of a small quantity of hydrogen in the internal rod atmosphere, the stoichiometry deviation is significantly reduced in the lower-powered rod of Fig. 10(a) (i.e., at 25 kW m^{-1}) relative to the higher-powered one of Fig. 10(b) (i.e., 52 kW m^{-1}). This result occurs because of the influence of the fuel temperature on the equilibrium stoichiometry deviation in Fig. 11. The equilibrium stoichiometry deviation in Fig. 11 has been evaluated with the Blackburn model of Appendix A.1.

Recently, a coulometric titration method has been used at the Chalk River Laboratories (CRL) to measure the O/U ratio of small samples taken from a spent CANDU fuel element that had defected in a commercial power reactor [38]. The element had a low burnup of 80 MWh/kgU and operated at a low power rating of 23–28 kW m^{-1}. Four samples (~100–200 mg per sample) were taken 6 cm from the primary defect location, where the primary defect had resulted from debris fretting. The average of the four samples yielded an O/U ratio of 2.044 ± 0.003, which is consistent with the low-power prediction of Fig. 10(a) (i.e., for a representative P_{H_2}/P_{H_2O} ratio of 0.1%). Unfortunately, the current technique did not permit information about the radial

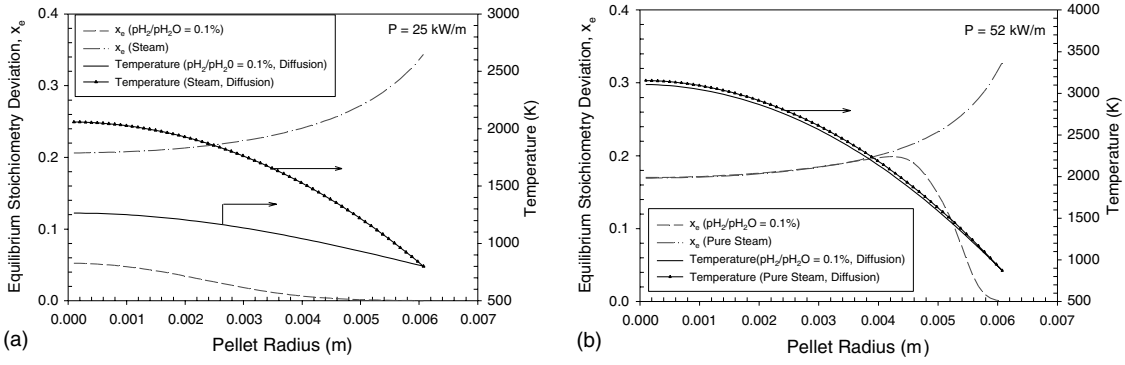

Fig. 11. Equilibrium stoichiometry deviation profile and temperature profile for different atmospheric oxygen potentials in the fuel-to-clad gap at (a) 25 kW m^{-1} and (b) 52 kW m^{-1}. The temperature profile accounts for the effect of oxygen diffusion in the fuel-to-clad gap.

location of the samples. Improved sampling methods at the CRL are currently being developed to obtain the O/U ratio as a function of the pellet radius [38].

3. Discussion

3.1. Fission product diffusion in defective rods

A methodology has been established to determine the fuel oxidation kinetics in operating defective rods. This oxidation process will directly enhance the fission product release as a consequence of a higher fuel temperature from a reduced thermal conductivity (Section 2.2.3) and a direct enhancement of the fission product diffusivity.

In accordance with the methodology of Ref. [21], the fission product release from the solid fuel matrix can be evaluated by integrating the release fraction over the fuel pellet radius. The release fraction in turn will depend on the diffusion coefficient D_{FP} (in $m^2\,s^{-1}$) for the fission products (FP) in the solid matrix which requires a specific knowledge of the fuel stoichiometry and temperature profile as detailed in Section 2.2.3 [21]. This coefficient is composed of three separate components that cover the low, intermediate and high temperature regimes as characterized, respectively, by the intrinsic, vacancy-enhanced (i.e., from radiation and fuel oxidation) and athermal mechanisms where [39]:

$$D_{FP} = 7.6\times10^{-10}\exp\left\{-\frac{35\,230}{T}\right\} + \left[\sqrt{2}\times10^{-25}\sqrt{\dot{F}}\exp\left\{-\frac{13\,890}{T}\right\} + x^2 2.22\times10^{-8}\exp\left\{-\frac{20\,230}{T}\right\}\right] + 2\times10^{-40}\dot{F} \quad (29)$$

in which $\dot{F}$ is the fission rate density (fission $m^{-3}\,s^{-1}$) and T is the fuel temperature (K). Thus, one can evaluate the solid-state diffusion coefficient (D_{FP}) for volatile fission products from the above formula with knowledge of the calculated fuel temperature and stoichiometry deviation profiles.

The oxygen partial pressure in the gap atmosphere must be known a priori to estimate the fuel oxidation state and fuel temperature. As an alternative approach, the fuel oxidation model can be used in a reverse fashion to determine the typical hydrogen-to-steam partial pressure ratio that must have existed in the gap to yield an observed fuel oxidation state in a given defective rod. For such an analysis, the natural defect experiment, FFO-102-2, is typical of an in-reactor hydride failure. This rod had operated at a high linear rating of 67 $kW\,m^{-1}$ in a high-pressure coolant of 100 atm. A post-test gravimetric analysis yielded a value of $x_e \sim 0.14$. Thus, using the fuel oxidation model of Section 2.2.3 (i.e., with oxygen diffusion), a value of $P_{H_2}/P_{H_2O} \sim 0.15\%$ is obtained to match the end-of-test equilibrium stoichiometry deviation (with a predicted value of $x_e \sim 0.17$). Moreover, with this ratio, the model is able to predict the observed melt radius for the high-powered FFO-102-2 rod.

This representative hydrogen-to-steam ratio can be used to investigate the effect of fuel oxidation on the fission product release. The model can be further tested against in-reactor sweep gas experiments (i.e., with non-oxidized CANDU fuel elements) and defect fuel experiments conducted at the Chalk River Laboratories (CRL) [3,40,41]. In particular, an empirical diffusivity (D'_{defect}) can be determined for defective fuel by scaling the sweep gas data by a correction factor H such that

$$D'_{defect} = HD'_{sweep\ gas}, \quad (30)$$

where

$$H = \left\langle \frac{D_{FP}(x,T)}{D_{FP}(0,T)} \right\rangle_{pellet}. \quad (31)$$

Here the diffusion coefficient D_{FP} is evaluated from Eq. (29) and H is obtained by averaging the oxidized-to-non-oxidized diffusion coefficient ratio over the fuel pellet volume (i.e., for the given temperature and fuel stoichiometry deviation profiles).

This methodology can be subsequently tested against the empirical diffusivity (D'_s) derived from a number of in-reactor defect experiments at the CRL [3]. For example, this comparison is shown for a low and high-powered rod in Table 1 where it is seen that the agreement is quite good (i.e., typically within a factor of 2).

3.2. Comparison to in-reactor experiments

As previously shown in Section 2.2.2, radiolysis does not appear to be an important consideration for the induction of fuel oxidation in defective rods where the Freundlich isotherm already yields rapid oxidation kinetics at high pressure (see Fig. 5). In fact, recent in-reactor experiments at Halden showed that irradiation of steam did not induce fuel oxidation in a closed system [17]. Although the hydrogen that is liberated in the radiolysis reaction can result in clad hydriding, this product may neutralize the tendency of its oxidizing counterparts to increase the stoichiometry of the fuel. Furthermore, as the temperature is raised, radiolytic effects should become insignificant to thermal effects as the thermal reactions and the recombination of transient species become faster.

The prediction that an equilibrium oxidation state is rapidly approached in defective rods is further supported (indirectly) by observations of the fission product release behaviour in in-reactor loop experiments at the Chalk River Laboratories [3].

Table 1
Empirical diffusion coefficient for defective fuel

Comparison with CRL experiments				
Linear power (kW m^{-1})	H[a]	$D'_{\text{sweep gas}}$ (s^{-1})[b]	D'_{defect} (s^{-1})[c]	D'_{s} (s^{-1})[d]
30	329	7.1×10^{-14}	2.3×10^{-11}	2.2×10^{-11}
60	2289	4.4×10^{-12}	1.0×10^{-8}	8.7×10^{-9}

[a] Evaluated from Eq. (31).
[b] Taken from Ref. [3].
[c] Evaluated from Eq. (30).
[d] Derived from the correlation in Ref. [41].

4. Conclusion

A model has been developed to describe the fuel oxidation kinetics in operating defective fuel rods. The model also considers the impact of the fuel oxidation behaviour on the degradation of the fuel thermal conductivity (i.e., due to the phonon and polaron contributions).

This model accounts for high-pressure oxidation in steam/hydrogen mixtures, based on Langmuir and Freundlich adsorption theory, and also considers radiolysis-assisted oxidation as a result of hydrogen peroxide production. Both isotherms predict a square root dependence on pressure from 0.01 to 1 atm in agreement with experimental data at 1473–1623 K. However, on extrapolation to high pressure (e.g., 100 atm), the predictions deviate where the Freundlich isotherm predicts faster kinetics which is in agreement with lower-temperature annealing experiments at 70 atm pressure. Furthermore, radiolysis does not appear to be an important consideration for the enhancement of the fuel oxidation kinetics in defective rods.

A stoichiometry profile will develop in defective rods under normal operation as a consequence of the temperature profile from the internal fission heating where the fuel oxidation thermodynamics are temperature dependent. This profile will tend to flatten out as a consequence of chemical diffusion of the interstitial oxygen ions in the solid. However, if this oxygen re-distribution process is ignored in the model, the profile determined solely by equilibrium thermodynamics is able to predict the observed occurrence of a dark band structure that may be due to the presence of a higher oxide phase (or perhaps gas bubbles). A measured radial profile of the stoichiometry deviation in a defective rod is needed to better understand and establish the oxygen transport effect in the model. However, during normal operating conditions, this uncertainty is not important from the perspective of the fission product release since the oxygen transport only affects the stoichiometry deviation in the outer region of the pellet where the temperature is lower, and hence the fission product release contribution is less significant.

Acknowledgements

The present work was supported by the Natural Sciences and Engineering Research Council of Canada, the Academic Research Program of the Department of National Defence (DND) and the Director General of Nuclear Safety of DND.

Appendix A. Oxygen partial pressure in the fuel and gap atmosphere

A.1. Oxygen partial pressure in the fuel

The oxygen partial pressure in the fuel as a function of x, i.e., $P_{O_2}(x)$ (in atm), is given by either the Blackburn thermochemical model [7]:

$$\ln P_{O_2} = 2\ln\left(\frac{x(2+x)}{1-x}\right) + 108x^2 - \frac{32\,700}{T} + 9.92 \tag{A.1}$$

or the solid solution representation of Lindemer and Bessman [8]:

$$P_{O_2} = \min(P_1, P_2), \tag{A.2}$$

where P_1 and P_2 are given by

$$\begin{aligned} \ln P_1 &= 2\ln\left(\frac{x(1-2x)^2}{(1-3x)^3}\right) - \frac{37\,621}{T} + 15.15, \\ \ln P_2 &= 4\ln\left(\frac{2x(1-2x)}{(1-4x)^2}\right) - \frac{43\,298}{T} + 25.74. \end{aligned} \tag{A.3}$$

A.2. Oxygen partial pressure in the gap

The oxygen potential in the gap atmosphere, P_{O_2} (in atm), is determined from the initial partial pressure of steam ($P^0_{H_2O}$) and hydrogen ($P^0_{H_2}$) in the fuel-to-clad gap, by solving the following cubic equation that results from mass balance considerations for the H and O in the gas mixture before and after steam dissociation [2,6]:

$$4(P_{O_2})^3 + 4[P^0_{H_2} - K^2_{H_2O}](P_{O_2})^2 + [(P^0_{H_2})^2 + 4P^0_{H_2O}K^2_{H_2O}]P_{O_2} - [(P^0_{H_2O})^2 K^2_{H_2O}] = 0. \quad (A.4)$$

The equilibrium constant K_{H_2O} is detailed in Eq. (5) as a function of temperature T.

References

[1] D.R. Olander, J. Nucl. Mater. 252 (1998) 121.
[2] B.J. Lewis, J. Nucl. Mater. 270 (1999) 221.
[3] B.J. Lewis, R.D. MacDonald, N.V. Ivanoff, F.C. Iglesias, Nucl. Technol. 103 (1993) 220.
[4] D.R. McCracken, Radiolytic effects in fuel degradation, AECL-11353, May 1995.
[5] D.R. Olander, W.E. Wang, Y. Kim, C.Y. Li, S. Lim, S.K. Suresh, in: Proc. Int. Top. Mtg. LWR Fuel Performance, Portland, Oregon, 2–6 March 1997.
[6] B.J. Lewis, B. Andre, B. Morel, P. Dehaudt, D. Maro, P.L. Purdy, D.S. Cox, F.C. Iglesias, M.F. Osborne, R.A. Lorenz, J. Nucl. Mater. 227 (1995) 83.
[7] P.E. Blackburn, J. Nucl. Mater. 46 (1973) 244.
[8] T.B. Lindemer, T.M. Besmann, J. Nucl. Mater. 130 (1985) 473.
[9] P.W. Atkins, Physical Chemistry, 5th Ed., WH Freeman and Company, New York, 1994.
[10] B.V. Dobrov, V.V. Likhanskii, V.D. Orzin, A.A. Solodov, M.P. Kissane, H. Manenc, J. Nucl. Mater. 255 (1998) 59.
[11] J. Albrefah, A. de Aguiar Braid, W. Wang, Y. Khalil, D.R. Olander, J. Nucl. Mater. 298 (1994) 98.
[12] D.R. Olander, Y.S. Kim, W. Wang, S.K. Yagnik, J. Nucl. Mater. 270 (1999) 11.
[13] B.J. Lewis, J. Nucl. Mater. 148 (1987) 28.
[14] J.M. Markowitz, Internal zirconium hydride formation in zircaloy fuel element cladding under irradiation, WAPD-TM-351, Bettis Atomic Power Laboratory, May 1963.
[15] J.C. Clayton, in: Proc. 8th Int. Symp. Zirconium in the Nuclear Industry, STP 1023, American Society for Testing and Materials, 1989, p. 266.
[16] D.R. Olander, S. Vakin, Secondary hydriding of defected zircaloy–clad fuel rods, EPRI TR-101773, 1993.
[17] D.R. Olander, W. Wang, Y.S. Kim, C. Li, K. Lim, Chemistry of defective light water reactor fuel, EPRI TR-107074, February 1997.
[18] J.F. Ziegler, J.P. Biersack, SRIM: the stopping and range of ions in matter, SRIM-2000 (v. 09), IBM-Research, Yorktown, New York, 1998.
[19] G.R. Choppin, J. Rydberg, Nuclear Chemistry Theory and Applications, Pergamon, Oxford, England, 1980, p. 311.
[20] A.W. Boyd, O.A. Miller, Can. J. Chem. 46 (1968) 3773.
[21] B.J. Lewis, F.C. Iglesias, D.S. Cox, E. Gheorghiu, Nucl. Technol. 92 (1990) 353.
[22] J.A. Meachen, Nucl. Energy 28 (4) (1989) 221.
[23] P. Ruello, L. Desgranges, G. Chirlesan, C. Petot, G. Petot-Ervas, Diffusion chimique dans le dioxyde d'uranium: cinetique en presence de clusters, unpublished work.
[24] D.R. Olander, Fundamental aspects of nuclear reactor fuel elements, TID-26711-P1, Atomic Energy Commission, 1976, p. 128.
[25] P.J. Reid, M.J. Richards, F.C. Iglesias, A.C. Brito, in: 5th International Conference on CANDU Fuel, ISBN 0-919784-48-8, Toronto, Ontario, vol. 1, 21–25 September 1997, p. 321 (Canadian Nuclear Society 1997).
[26] W.E. Ellis, J.D. Porter, T.L. Shaw, in: International Topical Meeting on Light Water Reactor Fuel Performance, Park City, Utah, 10–13 April 2000, p. 715.
[27] R.L. da Silva, Irradiation of a CANDU UO_2 fuel element with twenty-three machined slits cut through the zircaloy sheath, Atomic Energy of Canada Ltd. report, AECL-8260, September 1984.
[28] P.G. Lucuta, R.A. Verrall, Hj. Matzke, J. Nucl. Mater. 223 (1995) 51.
[29] V.C. Howard, T.F. Gulvin, UKAEA Report, IG Report 51 (RD/c), 1961.
[30] L.A. Goldsmith, J.A.M. Douglas, J. Nucl. Mater. 47 (1973) 31.
[31] P.G. Klemens, Phys. Rev. 119 (2) (1960) 507.
[32] P.G. Klemens, High Temp.–High Press. 17 (1985) 41.
[33] P.G. Klemens, Proc. Phys. Soc. (Lon.) A 68 (1955) 1113.
[34] R.A. Gomme, J.C. Carrol, T.L. Shaw, High Temp.–High Press. 30 (1998) 135.
[35] P.W. Winter, J. Nucl. Mater. 161 (1989) 38.
[36] P.J. Reid, M.J. Richards, SOURCE 2.0 software theory manual and design description document: fuel heat capacity, Ontario Power Generation Report, File no. N 06631.01 P SOURCE Design Description 0.00 QA RSOAD, May 1997.
[37] M. Billaux, Siemens Power Corporation, private communication, September 2000.
[38] R.A. Verrall, J.F. Mouris, in: 7th International Conference on CANDU Fuel, ISBN 0-919784-71-2, Kingston, Ontario, vol. 2, 23–27 September 2001, p. 3A-1 (Canadian Nuclear Society 2001).
[39] B.J. Lewis, in: 6th International Conference on CANDU Fuel, ISBN 0-919784-62-3, Niagara Falls, Ontario, vol. 1, 26–29 September 1999, p. 403 (Canadian Nuclear Society 1999).
[40] I.J. Hastings, C.E.L. Hunt, J.J. Lipsett, R.D. Delaney, Short-lived fission product release from the surface and centre of operating UO_2 fuel, AECL-8353, Atomic Energy of Canada Limited (1984).
[41] B.J. Lewis, R.J. Green, C.W.T. Che, Nucl. Technol. 98 (1992) 307.